Original Article

SHM Structural Health Monitoring

Structural Health Monitoring
2016, Vol. 15(2) 223–234

DOI: 10.1177/1475921716636375
shm.sagepub.com
SAGE

Fast wavenumber measurement for accurate and automatic location and quantification of defect in composite

Olivier Mesnil[1], Hao Yan[2], Massimo Ruzzene[1,3], Kamran Paynabar[2] and Jianjun Shi[2]

Abstract

As the use of and dependence on composite materials is increasing in all industries, there is a strong need for reliable, accurate, and fast techniques for damage detection and quantification in composite plate-like structures. Among the various nondestructive evaluation and structural health monitoring techniques, many rely on Lamb wave long-range propagation. A wavenumber quantification technique called frequency domain instantaneous wavenumber has been previously proven to be an efficient technique to estimate in-plane (i.e. position) and out-of-plane (i.e. depth) coordinates of defects in composites. This paper further develops this technique by (1) reducing the acquisition time by one order of magnitude while improving the quality of detection, (2) implementing an automatic feature extraction process to automatically assess the geometry and obtain information which can be directly used for decision making, and (3) quantifying the cumulative error of the whole process.

Keywords

Guided waves, composite materials, structural health monitoring, damage assessment, nondestructive evaluation

1 Introduction

With the rising use of composite material in the aerospace industry, the need for efficient, fast, and reliable structural health monitoring (SHM) techniques has become increasingly important. Highly sensitive to defects invisible to the naked eye, Lamb waves, first described and identified by Lamb,[1] are the basis for various SHM and nondestructive evaluation (NDE) techniques. Reviews of defect detection and quantification techniques using guided waves can be found in Su et al.[2] and Raghavan and Cesnik.[3] Among these techniques, many use a laser doppler vibrometer (LDV) to measure Lamb waves induced by piezoelectric (PZT) transducers and deduce information about the health of the structure. A review of LDV-based methods is given in Sundaresan et al.[4] Significant research has been done since then and can be summarized as follows: Staszewski et al.[5] showed the potential of LDV-based method; Yu et al.[6] detected cracks in aluminum; Sohn et al.[7] detected delamination by extracting standing waves; Rogge and Leckey[8] estimated the depth of defects for both numerical and experimental data; Ostachowicz et al.[9] located notches in isotropic material using a three-dimensional LDV; and Flynn [10] detected defects using steady state ultrasonic vibration. Instead of using a PZT transducer, an air coupled transducer was used in Dhital et al.[11] coupled to LDV measurements to obtain a fully noncontact defect evaluation technique. Other techniques use PZT transducers for both actuation and measurement of Lamb wave for damage detection purposes and therefore make the economy of a laser vibrometer.[12–15] The frequency domain instantaneous wavenumber (FDIW) technique has been previously developed by the authors[16] as a technique using PZT excitation and full field LDV measurements to obtain in-plane (i.e. location) and

[1]D. Guggenheim School of Aerospace Engineering, Georgia Institute of Technology, USA
[2]H. Milton Stewart School of Industrial & Systems Engineering, Georgia Institute of Technology, USA
[3]W. Woodruff School of Mechanical Engineering, Georgia Institute of Technology, USA

Corresponding author:
Olivier Mesnil, D. Guggenheim School of Aerospace Engineering, Georgia Institute of Technology, Atlanta, GA, 30332, USA.
Email: omesnil3@gatech.edu

out-of-plane (i.e. depth) coordinates of defects in composites. In Mesnil et al.,[17] the authors show a first collaborative work resulting in an automatic feature extraction process relying on the Smooth Sparse Decomposition[18] (SSD) algorithm, which is a flexible defect detection technique to automatically separate the defect component from the background, based on the different spatial structure of each component.

Despite the development and constant improvement of the LDV-based defect detection techniques, very few are actually deployed in the industry. The reasons for this are many, including the reliability of the techniques, the overall efficiency, the cost, and the fact that those techniques provide so much information that the decision making process can be very challenging. Another obstacle to the implementation of these techniques in SHM is the measurement duration. The typical acquisition time of a wavefield to quantify a defect with an accuracy of the order of the millimeter using the FDIW technique is of the order of one to five hours for an area of 10×10 cm^2. Even if the technique provides excellent results, its acquisition time is a major constraint for its direct implementation. Although the simplest (and also the most costly) solution to resolve this issue would be to use a multi-beam laser vibrometer[19], measuring several pixels simultaneously with several laser beams, hence reducing the acquisition time by the number of beam, the authors believe that it is necessary for this technique to be significantly faster before being used in the industry.

In this paper, we overcome this acquisition time issue by speeding up the FDIW technique by one order of magnitude through measuring the steady state of vibrations in a composite plate in the frequency domain using a laser vibrometer with the option called "fast scan". Furthermore, the multi-modality of the Lamb wave was neglected in Mesnil et al.[16] because the A0 wavenumber was supposed to be dominant compared to the wavenumber of the S0 mode. In this paper, the modes are properly filtered, resulting in much more accurate defect maps. An uncertainty quantification procedure is also developed to construct confidence intervals around the point estimates. To achieve this goal, the initial noise variance and its propagation through the process are estimated. Moreover, after the estimation of the uncertainty of the wavenumber and the effective thickness maps, this estimation uncertainty can be used as an input for further defect isolation algorithm. The defect isolation algorithm is based on the SSD algorithm as proposed in Yan et al.,[18] which can accurately quantify the defect region.

The reduction of the inspection time of the FDIW technique allows online systematic monitoring of small structures or preselected critical regions of large structures more susceptible to develop anomalies and is a necessary step toward using full guided wave acquisition system such as LDVs for online SHM inspection of structures. The technique can also be used to monitor damage growth in a structure periodically loaded to study the fatigue phenomena. Furthermore, this technique is the data processing part of a hybrid SHM/NDE technique in which embedded sensors perform in-service damage detection while the LDV based technique is a ground-based technique providing additional information at the defect location, in order to give prediction regarding the remaining life of the structure. Alternatively, the FDIW technique is compatible with full field wave measurement acquired by established or emerging technologies such as air coupled transducers, electromagnetic acoustic transducer or digital image correlation cameras.

The remaining of the paper is organized as follows: the evolution of the FDIW into the fast wavenumber (FW) technique is first described in the next section. The post filtering technique and the automatic feature extraction algorithm are then presented in the third section. Finally the overall technique is applied to a more complex artificial defect and a real life impact defect in the fourth section.

2 Wavenumber quantification

In this section, for illustration purposes, a 61×61 cm^2 8 plies 1.6 mm thick quasi-isotropic fiber glass composite plate is studied. During the manufacturing of this plate, a 25.4 mm (1 inch) diameter thin Teflon disk was inserted between the second and the third ply to prevent layer bounding and simulate a delamination. Guided waves are excited by a PZT transducer glued at the center of the plate, at a distance of 10 cm from the center of the artificial delamination. The propagating Lamb waves are recorded with a laser vibrometer PSV-400. The excitation frequency ω_0 of the PZT is chosen such that only the first Lamb wave modes, A0 and S0, propagate through the specimen. A schematic of the experimental setup is shown in Figure 1. Dispersion relations of the specimen are computed using the semi analytical finite element (SAFE) method described in Bartoli et al.[20] The authors are well aware that this artificial defect may not be very representative of real delamination, but results with realistic defects will be presented in the "Results on complex real life defects" section.

2.1 Frequency domain instantaneous wavenumber and effective thickness

The FDIW is a wavenumber quantification tool previously developed by the authors[16] which relies on the instantaneous wave-vector analysis.[21] The main

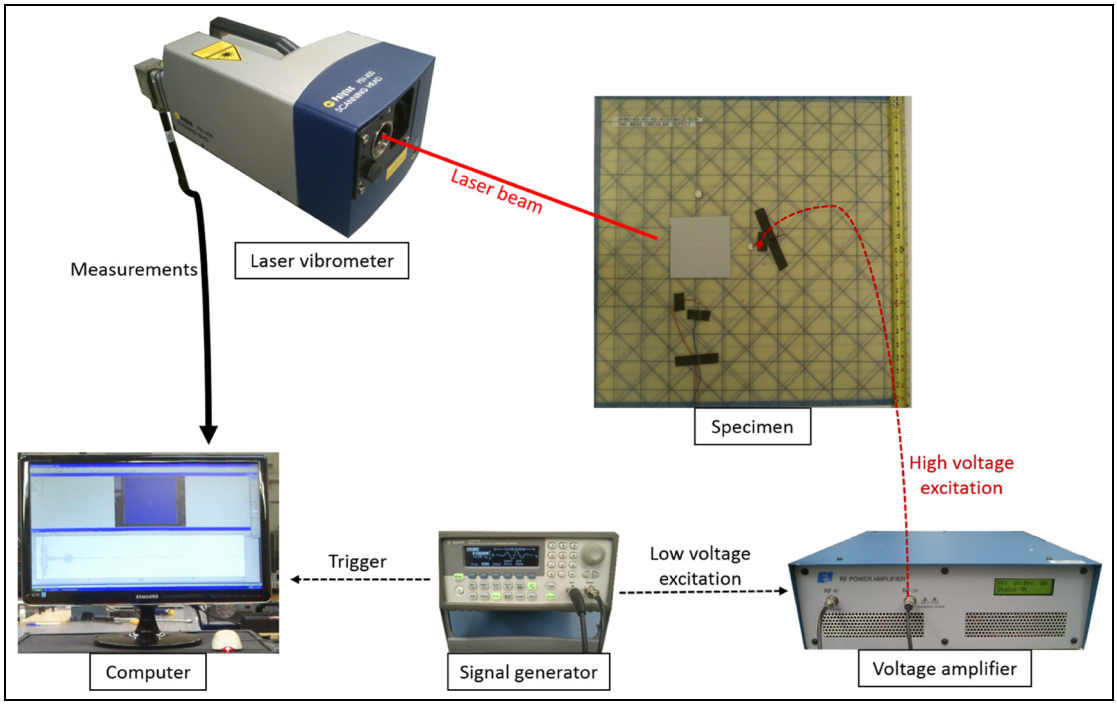

Figure 1. A schematic of the experimental setup. The excitation function is generated by a signal generator, amplified, and fed to a PZT to generate guided waves in the specimen. The out-of-plane velocity is recorded at a grid of points by the LDV and sent to a computer for analysis. The computer and the signal generator are synchronized so the measurement starts when the excitation function is sent.

definition and results are summarized in this section. Given a wavefield function of time and space $w(x,y,t)$ (i.e. the time evolution of the displacement of the pixel of coordinate (x,y)), the instantaneous wavenumber (IW), a local quantification of the wavenumber at each time frame of the wavefield, is computed by deriving spatially the phase of the analytical signal of the wavefield, where the analytical signal $g(x,y,t)$ of the wavefield is given by $g(x,y,t) = w(x,y,t) + i\mathcal{H}(w(x,y,t))$ where $\mathcal{H}$ denotes the Hilbert transform. To avoid computing and unwrapping the phase, an alternative computation is described by Rogge and Parker[22]

$$IW(x,y,t) = \mathrm{Im}\left(\frac{1}{g}\left(\left(\frac{\partial g}{\partial x}\right)^2 + \left(\frac{\partial g}{\partial y}\right)^2\right)^{1/2}\right) \quad (1)$$

$IW(x,y,t)$ is now the value of the wavenumber at the pixel (x,y) of the wavefield and at the time step t. As the wavenumber is more relevant if it is expressed as a function of the frequency, the IW is applied in the frequency domain, becoming the FDIW. Let $W_0(x,y)$ be the wavefield at the dominant frequency. W_0 is given by

$$W_0(x,y) = \mathcal{F}(w(x,y,t))|_{\omega_0} \quad (2)$$

where $\mathcal{F}$ denotes the Fourier transform and ω_0 is the excitation frequency. The FDIW is then defined by applying equation 1 to W_0 ignoring the time variable. Doing so has two main advantages. First, the quantity of information to deal with is much smaller, as the output of this process is a single picture (as for the traditional IW process, the output is a picture for every time step). Second, the wavenumber is now computed at a known frequency ω_0, which allows us to use the knowledge of the dispersion relations of the specimen to interpret the results and obtain an estimate of the depth of the defect.

The effective thickness is a local quantification of the depth of the defect equal to the number of undamaged layers between the scanned surface and the closer subsurface feature. In the case of a pristine plate, the effective thickness is equal to the number of layers of the plate (the closest subsurface feature is the other edge of the plate). For the 8-layer plate with artificial delamination studied in this section, the theoretical effective thickness takes a value of eight everywhere except at the Teflon disk location where the effective thickness takes a value of two (the Teflon disk was inserted between the second and the third ply with respect to the scanned surface). In order to obtain an estimate of the depth of the delamination, it is assumed

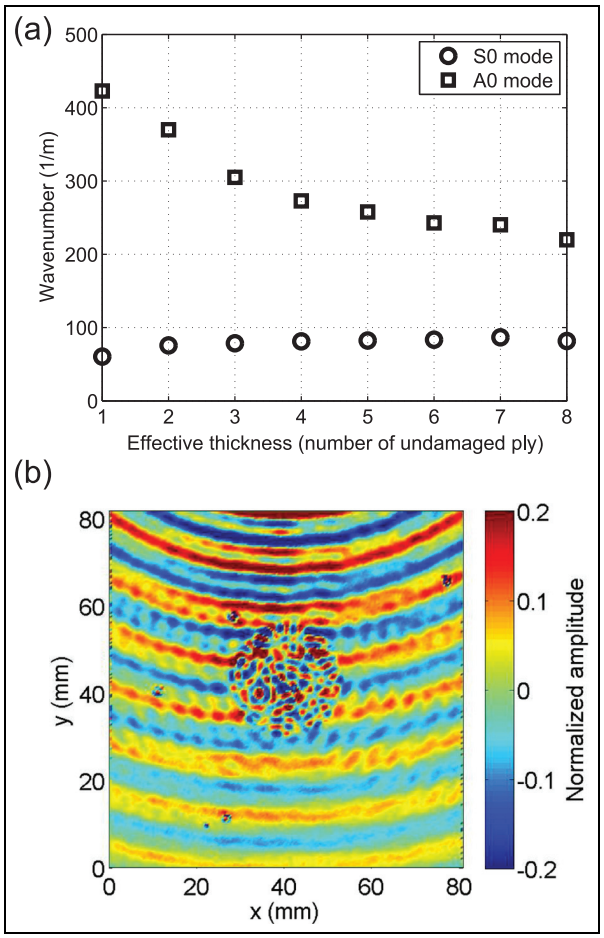

Figure 2. Application of the FDIW process to a delaminated area (Teflon disk inserted) in a glass fiber composite plate: (a) theoretical wavenumber as a function of the effective thickness (i.e. depth of the defect) for A0 (squares) and S0 (circles) modes; (b) frequency wavefield at 300 kHz.

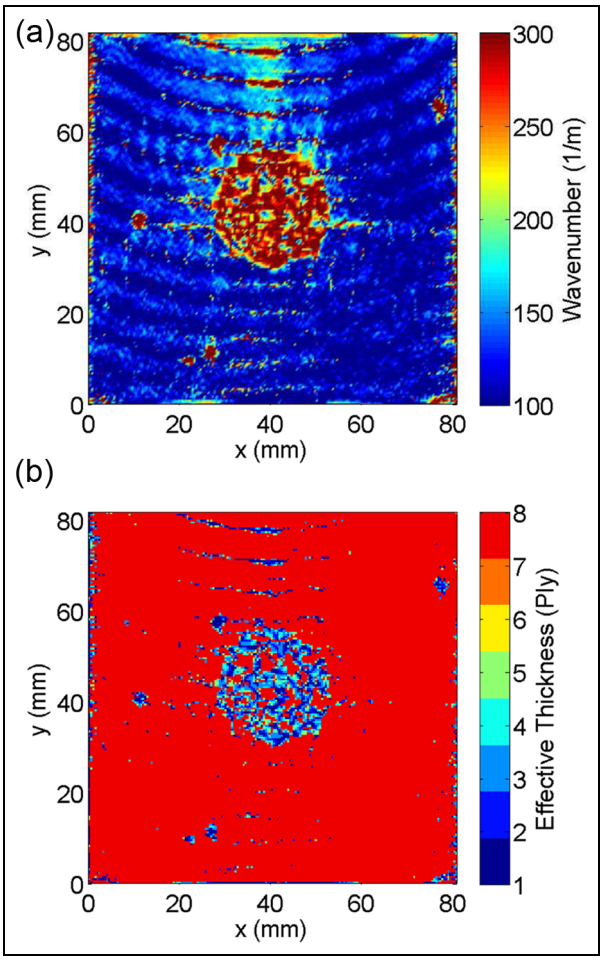

Figure 3. Application of the FDIW process to a delaminated area (Teflon disk inserted) in a glass fiber composite plate: (a) wavenumber map; (b) effective thickness map.

that the two undamaged layers between the scanned surface and the Teflon disk vibrate like a free composite plate. More generally, the dispersion relations are computed not only for the pristine plate, but also for all sets of upper layers (i.e. layer [1], layers [1,2], layers [1,2,3], etc.) with their corresponding layups. Note that the quasi-isotropy property does not hold for most sets of upper layers. The corresponding wavenumbers are stored and each pixel of the FDIW map is compared to this list of possible wavenumbers. The sequence of possible wavenumber values of both A0 and S0 modes are shown in Figure 2(a). As the variation of the wavenumber of the A0 mode as a function of the depth of the defect is greater than the one of the S0 mode (see Figure 2(a)), only the wavenumber of the A0 mode is considered in the rest of this section because its variation is easier to measure. At each pixel, the effective thickness value corresponding to the closer wavenumber match is stored to create the effective thickness map.

An example of the entire process is shown in Figures 2(b) to 3(b). The wavefield $w(x, y, t)$ used to generate Figures 2(b) to 3(b) is made of 200×200 pixels (area of 10×10 cm^2) and 512 time steps corresponding to a recording duration of 200 μs at each pixel. The excitation function is a 300 kHz 4-cycle sine burst. The time window is chosen such that no reflected wavepacket exists within the region of inspection during the duration of each measurement so that the plate is virtually infinite. At every pixel, the out-of-plane displacement is recorded 10 times and averaged in order to increase the signal to noise ratio. To total acquisition time for such a scan is of the order of three hours. The frequency wavefield W_0, the corresponding FDIW map and the effective thickness map are shown in Figures 2(b), 3(a), and 3(b), respectively. The measured delaminated area is a circle of diameter included within 25.5 to 26.2 mm while the actual delamination is a circle of diameter:

25.4 mm and the average effective thickness in the delaminated area is 2.52 (actual depth: two layers). The slight overestimation of the defect depth may be due to the fact that the Teflon disk does not behave like a void so the upper layers in the delaminated area do not vibrate freely because of the boundary condition with the Teflon disk.

Even though these results provide correct location, size, and depth estimates, the data acquisition time is very long (about three hours for this case) and a lot of information is wasted in the process of converting $w(x, y, t)$ to $W_0(x, y)$. Furthermore, in the frequency wavefield (Figure 2(b)) the modes A0 and S0 are superimposed, which results in the fact that the IW map (Figure 3(a)) is now a function of both A0 and S0 modes, and therefore converting it into the effective thickness map using the dispersion relations of the A0 mode is not a reliable operation. In this example, the wavenumber in the non-delaminated area of Figure 3(a) is included between 100 and 150 1/m while the theoretical wavenumbers of the $A0$ and the $S0$ modes in the pristine region are equal to 220 and 82 1/m respectively as shown in Figure 2(a). Thus, the wavenumber of the FDIW map in Figure 3(a) can be considered as a weighted averaged between the $A0$ and $S0$ wavenumbers, making it difficult to interpret. A single mode must therefore be extracted.

2.2 Wavenumber quantification by continuous excitation

A substantial amount of the acquisition time is spent on waiting for the toneburst wavefront to die out in the specimen before sending another toneburst and starting a new measurement. It must be reminded that in the previous scan, the 40,000 pixels are scanned 10 times each for averaging purposes. The out-of-plane displacement of each pixel is recorded during 400 μs, but a 10 ms delay should be condoned between toneburst impulses to dissipate the energy and wait for the specimen to be at rest.

2.2.1 Fast scan as a LDV option. The "fast scan" is an option of the LDV PSV-400. Instead of measuring the transient response of the propagating wave by a time acquisition, the steady state response of the system at one frequency is measured during a fast scan acquisition. To measure the steady state response of the plate, the PZT is continuously excited at a given frequency. At every scanned point, a fixed number of periods P is recorded by the LDV, then a fast Fourier transform (FFT) is applied to this data and only the complex value of this FFT at the excitation frequency is recorded by the computer. The operation is repeated for every point of the grid with no interruption in the excitation signal. Since the steady state response of the plate is measured, there is no need to wait for the plate to be at rest between each measurement, and therefore the acquisition of a fast scan is usually one or two orders of magnitude faster than a regular time scan. However, a fast scan is the single frequency response of the specimen and hence contains less information than a regular time scan, but can be used to compute a wavenumber value in a very similar way as was done with the FDIW. The same experimental setup as in the previous section is used. The PZT is continuously excited at 300 kHz. A hundred periods are used to compute the FFT values at every pixel, which results in a total computational time of approximately 10 minutes instead of three hours. The LDV is synchronized with the PZT so that all the measurements are in phase. Note that the fast scan is made of the incident wavepackets from the source as well as a nearly infinite number of reflected wavepackets from the edges and the features embedded in the specimen. Due to the complex behavior of the interaction of the multiple reflections, the reflected wavepackets can not be interpreted and contribute the noise of the measurement. As the fast scan wavefield is a complex quantity (as a result of a FFT for each pixel), only its real part is displayed in Figure 4(a), but both the real and imaginary parts are used in the data processing of the following sections. The spatial FFT of the fast wavefield, corresponding to the 300 kHz frequency slice of the dispersion relations is also shown in Figure 4(b), where the spatial wavenumbers k_x and k_y are the representation of the coordinate axis x and y in the Fourier domain. Note that the position of the actuator with respect to the defect is of very little importance as long as the amplitude of the wavepackets within the region of interest is sufficient to achieve an appropriate signal to noise ratio.

2.2.2 Mode extraction. As was previously the case with the FDIW, the fast scan wavefield is the superposition of both the A0 and S0 modes. A single mode must be extracted in order to obtain a reliable wavenumber quantification. The A0 mode is chosen for this analysis as the variation of the A0 mode as a function of effective thickness is greater than the one of the S0 mode (see Figure 2(a)), which will result in an easier detection. Furthermore, reflection on the edges and backward propagation of both modes are also filtered. Tools for mode separation have been developed in Ruzzene[23] and Michaels et al.[24] In order to filter the A0 mode, and keep the wavenumber corresponding to the delaminated area, all the wavenumbers not in the 100 to 450 rad/m range in the downward propagating direction are

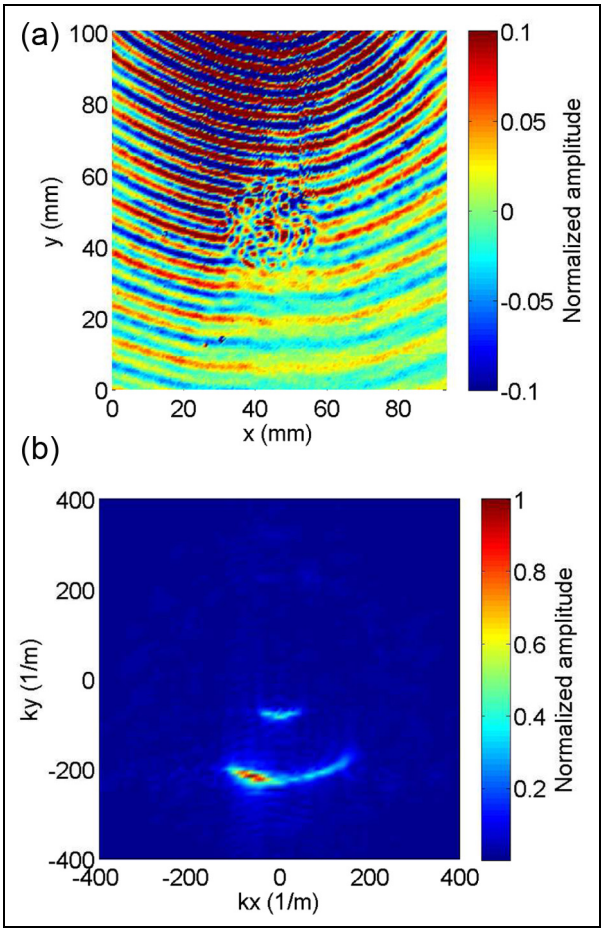

Figure 4. (a) Real part of a fast wavefield at 300 kHz measured from a delamination (Teflon disk inserted) in glass fiber. (b) Corresponding dispersion relations at 300 kHz where both modes (A0 & S0) can be observed.

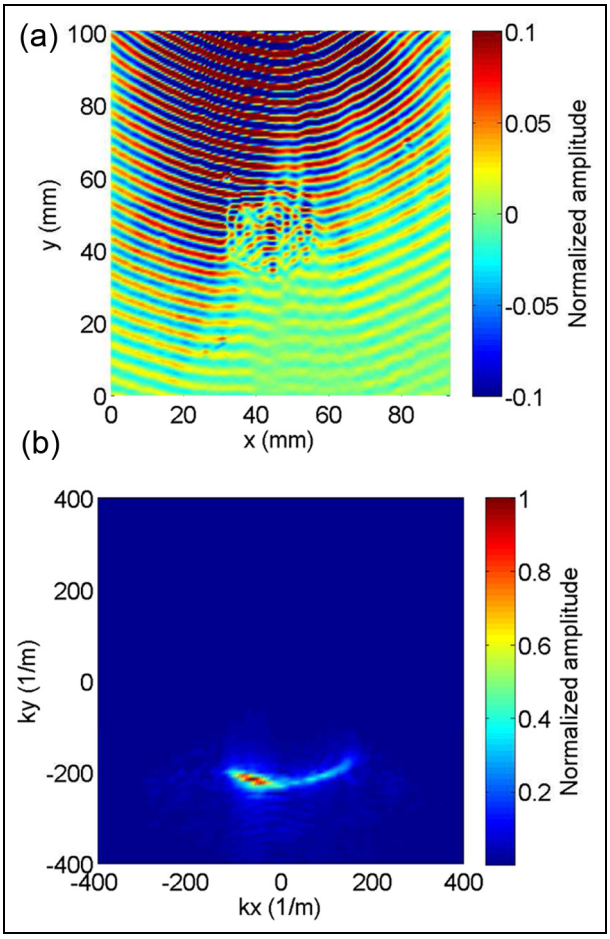

Figure 5. (a) Real part of a fast wavefield at 300 kHz measured from a delamination (Teflon disk inserted) in glass fiber after filtering out the S0 mode. (b) Corresponding dispersion relations at 300 kHz where only the A0 mode is left.

filtered out. The bounds of the range of frequencies to keep are determined using Figure 2(a) making sure that the S0 mode is removed, but all possible A0 wavenumbers are kept intact. The A0 only wavefield and its dispersion relations are displayed in Figures 5(a) and 5(b).

2.2.3 Wavenumber measurement. As the fast scan wavefield is already a complex quantity, there is no need for the Hilbert transform anymore since it is only used in the FDIW process to obtain a phase quantity. The FW is simply computed by taking the quadratic norm of the gradient of the phase of each pixel of the fast scan wavefield

$$FW(x,y) = \| \nabla ph(x,y) \|_2 \qquad (3)$$

where $ph(x,y)$ is the phase at every pixel of the recorded wavefield. The phase is computed using the integrated one-dimensional phase unwrapping command of Matlab for every line and column of the wavefield. It has been chosen to use the phase instead of using a similar expression to equation 1 in order to be able to apply some pre-processing filters to the phase.

Alternatively one may apply a two-dimensional phase unwrapping algorithm, such as the ones developed in Ghiglia and Pritt,[25] to the Fast Scan. However, this process is computationally much slower and does not provide more accurate results. Indeed, two-dimensional phase unwrapping techniques provide the absolute value of the phase at any point relative to an origin point. Therefore the phase computed with two-dimensional techniques differs only an additive constant compared to the one-dimensional unwrapping phase technique. As the phase is immediately derived, the knowledge of this additive constant is not useful.

As the first-order spatial derivative of the phase is computed in order to obtain the wavenumber value (equation 3), the measurement noise is amplified. To reduce the impact of the noise, the phase is preprocessed by an average filter: the phase of every pixel is equal to

the average of the phase of the surrounding pixels. The number of pixels used for the averaging operation, denoted by N, influences the quality of the wavenumber estimate. If N is too small, the noise is not efficiently removed. For N too large, the phase would be so smooth that no defect could be detected. Experimentally, N is chosen such that the smoothing is done over half the wavelength of the A0 mode of the pristine plate. For this experimental setting, $N = 5$ pixels is chosen, corresponding to an average phase filter on 2.5 mm. The FW map and the effective thickness estimation corresponding to Figure 5 (A0 mode only) is shown in Figures 6(a) and 6(b), respectively.

At first glance, the result of Figure 6(b) is better than the one of Figure 3(b) because the circular shape is estimated much more precisely. The overall picture obtained by the fast scan technique is more noisy than the one obtained by the traditional FDIW technique due to the small value of N, before the derivation of the phase. The estimated delamination is a circle of diameter included between 26.3 and 27.9 mm for an average depth of 2.6 layers. The most noticeable difference between Figure 3(b) and Figure 6(b) is that the full circular delamination is estimated thanks to the mode filtering unlike in the previous results which presented a non-fully delaminated area (Figure 3(a)). In addition to providing a better overall defect mapping, the acquisition time for the Fast Scan is around 10 minutes.

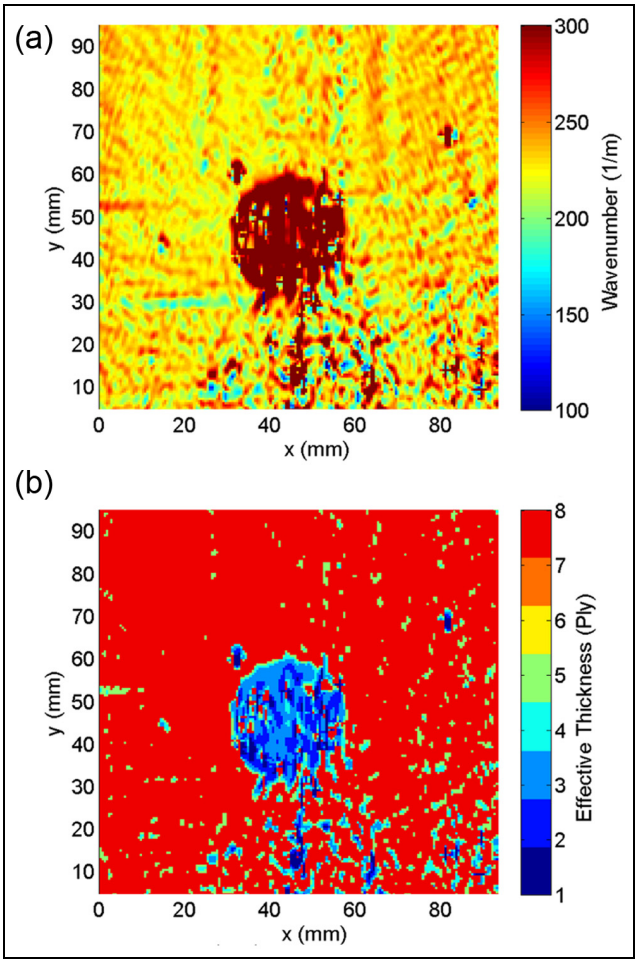

Figure 6. (a) FW map corresponding to Figure 5(a) and (b) the corresponding effective thickness map.

3 Post filtering technique and features extraction

In the previous section, an estimate of the effective thickness map has been obtained. However, there are two additional challenges that should be addressed before this technique can be used in practice. First, the procedure described earlier only gives point estimation for the effective thickness, and no information about the estimation uncertainty is provided. Second, the effective thickness estimation contains random noise, even after the filtering technique was applied, which affects the clear defect region quantification and exact extraction of the defect location. Consequently, in this section, we first develop an uncertainty quantification technique to model the variance propagation throughout the entire process, and then we implement an automatic defect identification technique called SSD, which can achieve fast and automatic denoising and defect detection for guided wave experiments.

3.1 Estimation uncertainty and confidence interval

This section is dedicated to the estimation of the uncertainty of the process and the evolution of the variance through the entire process. Variance propagation is a phenomenon that occurs during nonlinear transformations, for example, for a sequential process, the noise of the previous steps would affect the estimation uncertainty in the following step. Consequently, we provide an uncertainty quantification procedure to accurately keep track of the uncertainty at each step.

To begin with, we provide a 95% confidence interval on the phase $ph(x, y)$ at every pixel of the recorded wavefield. Since the one-dimensional phase unwrapping algorithm is applied to each column and each row of the wavefield, we use a standard deviation with a window of size $N = 5$ to estimate the standard deviation $\sigma_x(x, y)$ of the pixel (x, y) in the x direction and $\sigma_y(x, y)$ in the y direction. The smoothed phase of a column of the wavefield and its first-order differential along with the corresponding 95% confidence interval is shown in Figure 7(a). The standard deviation of the fast scan wavefield σ_{FW} is estimated by

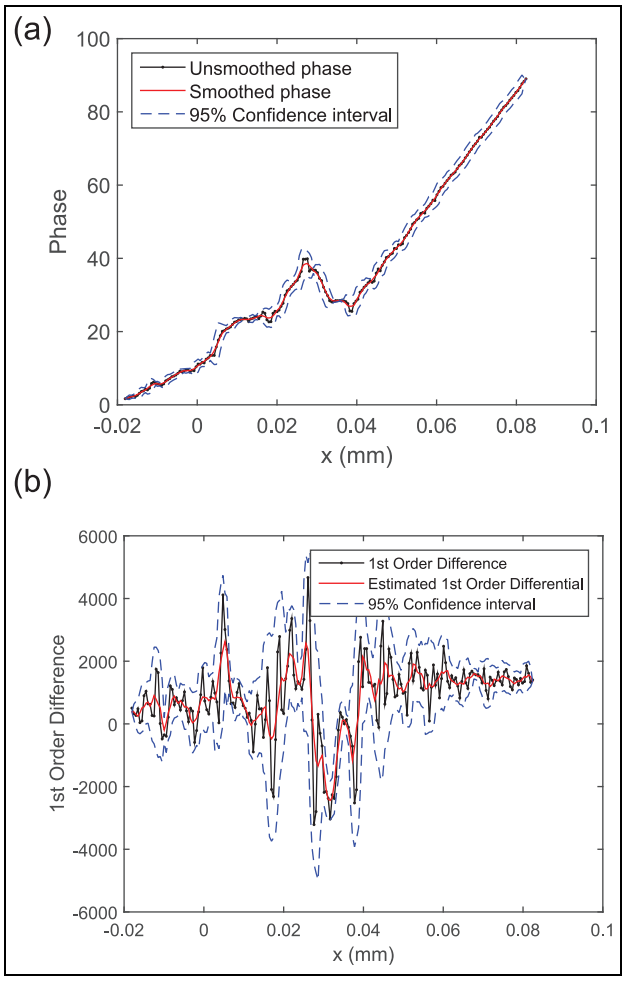

Figure 7. Phase of a line of the wavefield: (a) original phase (black dashed line), smoothed phase (red solid), and 95% confidence interval (blue dashed line); (b) first-order differentials of the phase corresponding to Figure 7(a).

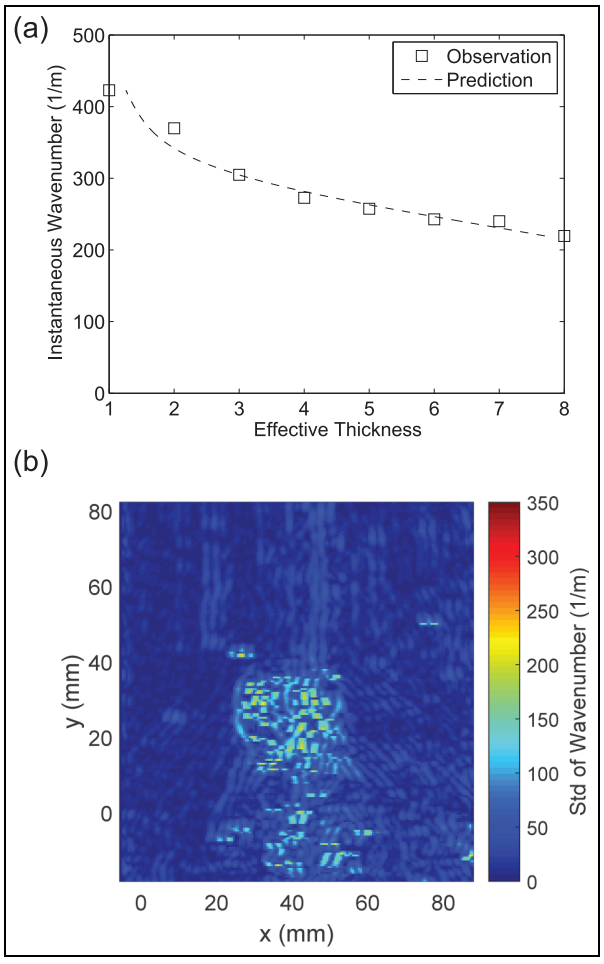

Figure 8. (a) Gaussian process model of dispersion relationship $f(k)$. (b) Standard deviation of the effective thickness σ_{ET}.

$$\sigma_{FW} = \sqrt{\left(\frac{\partial ph(x,y)}{\partial x}\right)^2 \sigma_x(x,y)^2 + \left(\frac{\partial ph(x,y)}{\partial y}\right)^2 \sigma_y(x,y)^2} \tag{4}$$

where $\frac{\partial ph(x,y)}{\partial x}$ and $\frac{\partial ph(x,y)}{\partial y}$ are the first-order differential of the phase along the x and y directions.

After the estimation of the standard deviation of the FW map σ_{FW}, the following step is to estimate the standard deviation of the effective thickness map σ_{ET}. As discussed in the previous section, the effective thickness map is obtained by converting a wavenumber value k using a function $f(k)$ computed by SAFE [20] corresponding to Figure 2(a). To estimate the variance propagation caused by a certain nonlinear transformation $f(k)$, the delta method[26] is then applied. The delta method is normally used for estimation of the variance of distribution after certain transformation. Consequently, σ_{ET} can be estimated by

$$\sigma_{ET} = \| f'(w) \| \sigma_{FW} \tag{5}$$

To estimate σ_{ET}, first, the Gaussian process model[27] is used to obtain an accurate estimation of both $f(k)$ and its first-order derivative $f'(k)$. The Gaussian process is normally used for meta-modeling estimation for computer experiments, for example, the finite element model (FEM), because of its ability to accurately estimate an entire curve based on a few measurement points. In this case, the entire dispersion relationship curve is estimated by a small number of points in the FEM. The estimation result of $f(k)$ is shown in Figure 8(a) and σ_{ET} is shown in Figure 8(b). Figure 8(a) shows the transformation from IW to effective thickness. It is clear from this figure that when the effective thickness is between layers 5 to 8, the first-order differential $f'(k)$ will be larger and consequently, from equation (5), we know that the estimation standard deviation σ_{ET} will also be larger. This implies that a defect located between layer 5 to layer 8 is not distinguishable from

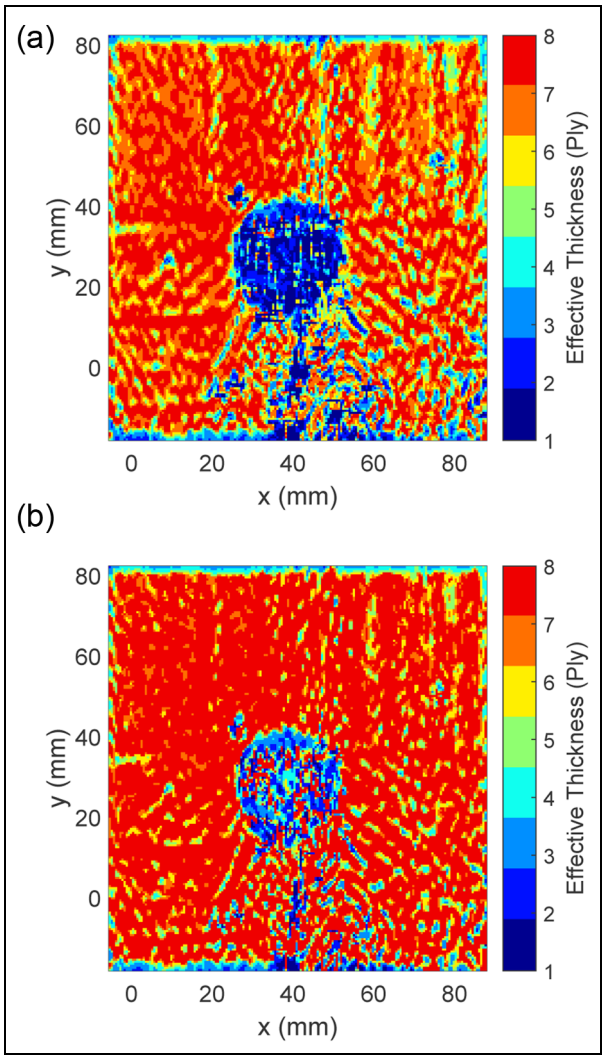

Figure 9. 95% confidence interval of the effective thickness map: (a) lower bound of 95% confidence interval; (b) higher bound of 95% confidence interval.

our estimation. From Figure 8(b), we can see that the following two areas have larger estimation uncertainty: one is the defect circle and the other is the area below the defect circle. The reason is that the phase of these two areas is nonsmooth, which increases the variance of the first-order differential.

Furthermore, the lower and higher boundary of 95% confidence intervals are also provided in Figures 9(a) and 9(b), respectively. From both Figure 9(a) and 9(b), it is clear that the circle is in the defect area and effective thickness is between two to three. Moreover, from Figure 9(b), which is the wavenumber map of higher 95% confidence interval, we can conclude that the area below the circle is probably not a defect because the effective thickness of this area is very similar to the background area.

3.2 Defect isolation

After the estimation of the 95% confidence interval of the effective thickness map, the following step is to isolate the defect region from the background. To achieve this, the SSD algorithm[18] is applied to detect and separate delaminations from the background of the FW map obtained in the previous step. The idea of the SSD algorithm is to decompose a noisy picture Y into three components: a smooth background (Y_B), irregular regions (corresponding to the delaminated regions (S)), and the measurement noise (E). To quantify different spatial structures of background, both the backgrounds and delaminated regions are represented by two bases, B and B_S, respectively. This leads to a decomposition as follows: $Y = Y_B + S + E = B\theta + B_S\theta_S + E$, where θ and θ_S are the basis coefficients corresponding to B and B_S, respectively. In addition, we assume that the representation of the defect S in the basis B_S is sparse. This assumption comes from the basic principle of compressive sensing and is normally valid because many natural signals and images are sparse or compressible in the sense that they have concise representation when expressed in a proper basis. Under these assumptions, this separation problem can be formalized as a penalized least square problem in equation 6 to get an accurate estimation of θ and θ_S

$$\begin{aligned} &\text{argmin}_{\theta,\theta_S} \parallel e\parallel^2 + \lambda\theta^{\mathrm{t}}R\theta + \gamma|\theta_S|_1 \quad \text{s.}t. \\ &Y = B\theta + B_S\theta_S + E \end{aligned} \tag{6}$$

where R is the roughness matrix, λ and γ are tuning parameters, and θ^{t} denotes the transpose of θ. The L_2 penalty term $\lambda\theta^{\mathrm{t}}R\theta$ regularizes the level of the mean smoothness, while the L_1 penalty term $\gamma|\theta_S|_1$ encourages the sparsity of defects. Since the formulation is convex, the accelerated proximal gradient algorithm[28] is applied in this setup because it is very efficient in high dimensional settings. More details such as algorithm formulation and tuning parameter selection can be found in Yan et al.[18]

The bases for the background and defect are selected based on the fact that the guided wave can only detect a defect size larger than half the wavelength. Consequently, the number of bases should be large enough to capture the window size of one-half the wavelength. In the experimental dataset, we use 3×3 spline basis B for background, and 25×20 spline basis B_S for the defect part. The estimation result is shown in Figure 11(a).

4 Results on complex real life defects

The complete process to obtain qualitative and quantitative defect information from a fast scan wavefield is

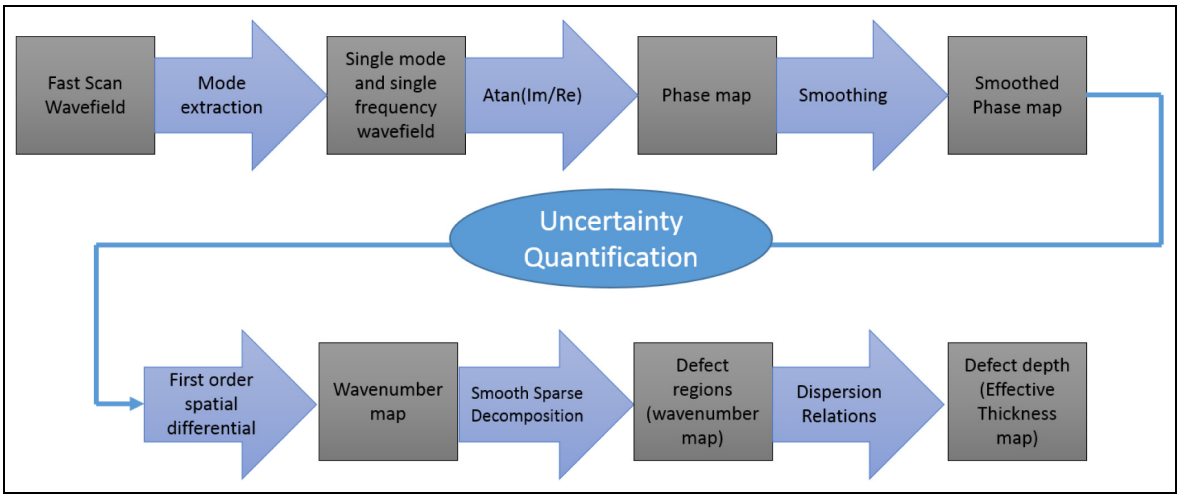

Figure 10. Schematic of the complete process to obtain the location and depth of defects from a fast scan wavefield.

the following. First, the modes are separated and extracted from the fast scan wavefield ("Mode extraction" section), then the phase map is computed, smoothed using an averaging filter and derived to obtain a wavenumber map ("Wavenumber measurement" section), the uncertainty is also quantified at this stage ("Estimation uncertainty and confidence interval" section). The defect regions are then isolated using the SSD algorithm ("Defect isolation" section). The wavenumber map is then converted in an Effective map using the media dispersion relations (if available) in order to quantify the depth of the defects ("Wavenumber measurement" section). The complete sequential process is described in Figure 10(a).

In this section, the complete process is being applied to more complicated defect geometries. The first complex defect geometry considered is a 61×61 cm^2 1 mm thick carbon fiber reinforced polymer (CFRP) panel. A 20 mm long peanut shape Teflon object was inserted inside the composite during the manufacturing. The exact through-the-thickness location of the Teflon object is unknown. The area of concern is a 12×10 cm^2 area and is scanned using a fast scan at 150 kHz. The fast wavefield is filtered to extract the A0 mode as detailed in the "Mode extraction" section. The wavenumber and the effective thickness maps are then generated and the feature extraction process is applied to generate Figure 11(b). The peanut shape is clearly visible in Figure 11(b) and the object seems to have been inserted between the second and the third layers.

The second geometry is a 122×61 cm^2 3.2 mm thick glass fiber plate. The defect was created by dropping a 1 kg mass on the plate from a height of 2 m. The impact area is a circle of 10 mm diameter. The previously developed process is applied to a fast scan recorded at 80 kHz on an area of 13×17 cm^2. The wavenumber map is displayed in Figure 11(c). Unfortunately, as the physical properties of this glass fiber plate (such as layup, fiber volume fraction, etc.) were not made available by the supplier, the dispersion relations of the media cannot be computed, and therefore no effective thickness map can be computed. However, the SSD process can still be applied to the wavenumber map and the circular area of defects since the impact is clearly visible in Figure 11(c).

5 Conclusion

In this paper, the FDIW technique was successfully upgraded to the a fast scan wavenumber technique by using a single frequency dataset instead of the complete time dependent wavefield, reducing the typical data acquisition time by one order of magnitude and increasing the reliability of the defect quantification. The uncertainty of the technique was studied by analyzing the deviation of the effective thickness map. An automatic defect detection process using the SSD algorithm was then developed and applied, and the cumulative error of the process was quantified. The validity of the process was confirmed by applying it to three experimental cases providing an accurate defect size and depth quantification. The output of the process is an effective thickness map, containing information about the health of the structure at every pixel of the studied area, which can be fed into a decision making program.

Funding

The work is funded by a collaborative agreement (NRANNH11ZEA001N VSST1) between NASA LaRC and

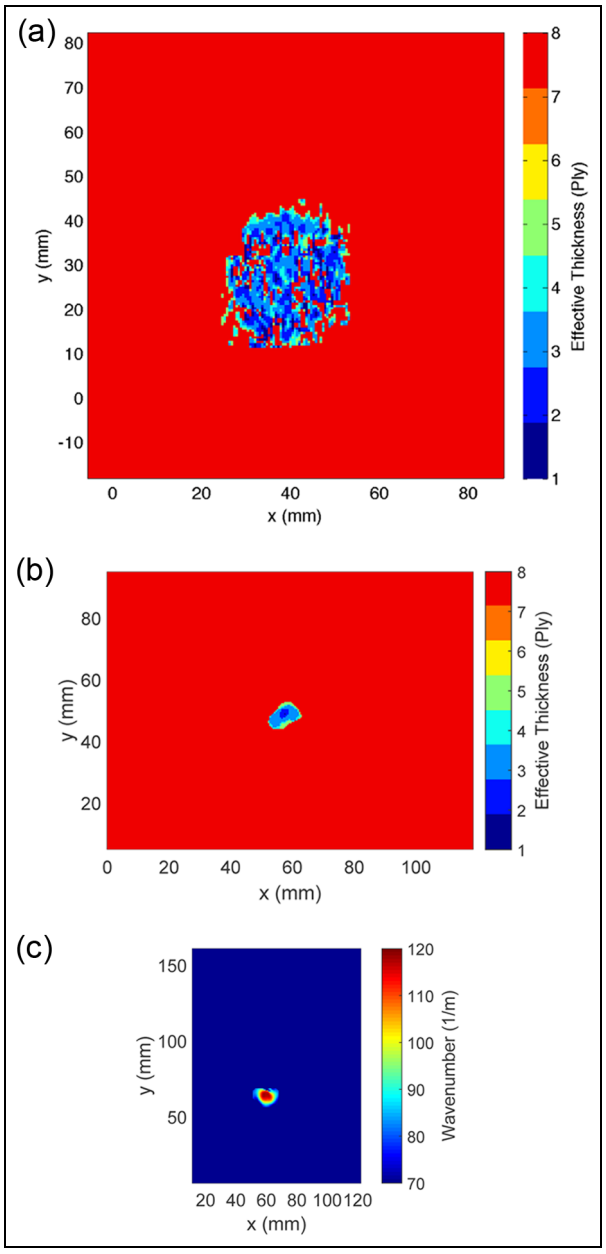

Figure 11. Feature extracted by the SSD algorithm: (a) effective thickness map for a glass fiber panel with a Teflon disk object inserted; (b) effective thickness map for a CFRP panel with a Teflon peanut shape object inserted; (c) wavenumber map for a glass fiber panel after impact by mass drop.

Georgia Tech and the Strategic University Partnership between Boeing and Georgia Tech.

References

1. Lamb H. On waves in an elastic plate. *Proc R Soc London Ser A* 1917; 93(648): 114–128.
2. Su Z, Ye L and Lu Y. Guided lamb waves for identification of damage in composite structures: A review. *J Sound Vib* 2006; 295(3): 753–780.
3. Raghavan A and Cesnik CE. Review of guided-wave structural health monitoring. *Shock Vib Dig* 2007; 39(2): 91–116.
4. Sundaresan M, Pai P, Ghoshal A, et al. Methods of distributed sensing for health monitoring of composite material structures. *Composites Part A* 2001; 32: 1357–1374.
5. Staszewski W, Lee B, Mallet L, et al. Structural health monitoring using scanning laser vibrometry: I. lamb wave sensing. *Smart Mater Struct* 2004; 13(2): 251.
6. Yu L, Leckey CA and Tian Z. Study on crack scattering in aluminum plates with Lamb wave frequency-wavenumber analysis. *Smart Mater Struct* 2013; 22(6): 065019.
7. Sohn H, Dutta D, Yang J, et al. Automated detection of delamination and disbond from wavefield images obtained using a scanning laser vibrometer. *Smart Mater Struct* 2011; 20(4): 045017.
8. Rogge MD and Leckey CA. Characterization of impact damage in composite laminates using guided wavefield imaging and local wavenumber domain analysis. *Ultrasonics* 2013; 53(7): 1217–1226.
9. Ostachowicz W, Wanddowski T and Malinowski P. Damage detection using laser vibrometry. In: *2nd international symposium on NDT in aerospace*, 22 November 2010, pp. 1–8.
10. Flynn EB. Embedded multi-tone ultrasonic excitation and continuous-scanning laser doppler vibrometry for rapid and remote imaging of structural defects. In: *EWSHM-7th European workshop on structural health monitoring*, Nantes, France, July 2014, pp. 1561–1567.
11. Dhital D, Lee JR, Park CY, et al. Laser excitation and fully non-contact sensing ultrasonic propagation imaging system for damage evaluation. In: *SPIE smart structures and materials+ nondestructive evaluation and health monitoring*, 26 April 2012, pp. 83430D.
12. Yan F, Royer RL and Rose JL. Ultrasonic guided wave imaging techniques in structural health monitoring. *J Intell Mater Syst Structs* 2010; 21(3): 377–384.
13. Valdes SHD and Soutis C. Real-time nondestructive evaluation of fiber composite laminates using low-frequency lamb waves. *J Acoust Soc Am* 2002; 111: 2026.
14. Michaels JE. Detection, localization and characterization of damage in plates with an in situ array of spatially distributed ultrasonic sensors. *Smart Mater Struct* 2008; 17(3): 035035.
15. Clarke T, Cawley P, Wilcox PD, et al. Evaluation of the damage detection capability of a sparse-array guided-wave SHM system applied to a complex structure under varying thermal conditions. *IEEE Trans Ultrason Ferroelectr Freq Control* 2009; 56(12): 2666–2678.
16. Mesnil O, Leckey CA and Ruzzene M. Instantaneous and local wavenumber estimations for damage quantification in composites. *Struct Health Monit* 2014; 14(3): 193–204.
17. Mesnil O, Yan H, Ruzzene M, et al. Frequency domain instantaneous wavenumber estimation for damage quantification in layered plate structures. In: *EWSHM-7th European workshop on structural health monitoring*, Nantes, France, July 2014, pp. 2338–2345.

18. Yan H, Paynabar K and Shi J. Image Smoothing and Anomaly Detection Via Smooth-Sparse Decomposition, 2015. Private communication.
19. Cupido E, Morel S and Smith D. Multipoint laser doppler vibrometer for transient analysis. In: *Proceedings of IMAC XXI*, Orlando, FL, 2003.
20. Bartoli I, Marzani A, Lanza di Scalea F, et al. Modeling wave propagation in damped waveguides of arbitrary cross-section. *J Sound Vib* 2006; 295(3): 685–707.
21. Stockwell RG, Lowe RP and Mansinha L. Instantaneous wave-vector analysis. In: *AeroSense'97*, 3 April 1997, pp. 349–358.
22. Rogge MD. Instantaneous wavenumber estimation of guided wavefield images for characterization of damage in composite structures. Report, NASA, Report no. NASA/TM-2013 (received via private communication from author), 2013.
23. Ruzzene M. Frequency–wavenumber domain filtering for improved damage visualization. *Smart Mater Struct* 2007; 16(6): 2116.
24. Michaels TE, Michaels JE and Ruzzene M. Frequency–wavenumber domain analysis of guided wavefields. *Ultrasonics* 2011; 51(4): 452–466.
25. Ghiglia DC and Pritt MD. *Two-dimensional phase unwrapping: Theory, algorithms, and software*. New York: Wiley, 1998.
26. Oehlert GW. A note on the delta method. *Am Stat* 1992; 46(1): 27–29.
27. Rasmussen CE. Gaussian processes in machine learning. In: *Advanced lectures on machine learning*, 2004, pp. 63–71. Berlin: Springer Berlin Heidelberg.
28. Parikh N and Boyd SP. Proximal algorithms. *Found Trends Optim* 2014; 1(3): 127–239.